JOURNAL OF APPLIED CRYSTALLOGRAPHY

ISSN: 1600-5767

journals.iucr.org/j

Quantifying radiation damage in biomolecular small-angle X-ray scattering

Jesse B. Hopkins and Robert E. Thorne

J. Appl. Cryst. (2016). **49**, 880–890

JOURNAL OF APPLIED CRYSTALLOGRAPHY

ISSN 1600-5767

Quantifying radiation damage in biomolecular small-angle X-ray scattering

Jesse B. Hopkins[a]* and Robert E. Thorne[b]

[a]Cornell High Energy Synchrotron Source, Ithaca, NY 14853, USA, and [b]Department of Physics, Cornell University, Ithaca, NY 14853, USA. *Correspondence e-mail: jbh246@cornell.edu

Received 24 November 2015
Accepted 25 March 2016

Edited by D. I. Svergun, European Molecular Biology Laboratory, Hamburg, Germany

Keywords: small-angle X-ray scattering; SAXS; radiation damage.

Supporting information: this article has supporting information at journals.iucr.org/j

Small-angle X-ray scattering (SAXS) is an increasingly popular technique that provides low-resolution structural information about biological macromolecules in solution. Many of the practical limitations of the technique, such as minimum required sample volume, and of experimental design, such as sample flow cells, are necessary because the biological samples are sensitive to damage from the X-rays. Radiation damage typically manifests as aggregation of the sample, which makes the collected data unreliable. However, there has been little systematic investigation of the most effective methods to reduce damage rates, and results from previous damage studies are not easily compared with results from other beamlines. Here a methodology is provided for quantifying radiation damage in SAXS to provide consistent results between different experiments, experimenters and beamlines. These methods are demonstrated on radiation damage data collected from lysozyme, glucose isomerase and xylanase, and it is found that no single metric is sufficient to describe radiation damage in SAXS for all samples. The radius of gyration, molecular weight and integrated SAXS profile intensity constitute a minimal set of parameters that capture all types of observed behavior. Radiation sensitivities derived from these parameters show a large protein dependence, varying by up to six orders of magnitude between the different proteins tested. This work should enable consistent reporting of radiation damage effects, allowing more systematic studies of the most effective minimization strategies.

1. Introduction

Small-angle X-ray scattering (SAXS) provides a low-resolution structural probe for biological macromolecules in solution. SAXS measurements generally require a homogeneous, monodisperse, aggregate-free solution, and that these conditions be maintained throughout data collection (Meisburger *et al.*, 2013). X-ray-induced radiation damage can cause macromolecule aggregation, fragmentation, conformation changes and unfolding, all of which can be detected by SAXS. Radiation damage is therefore a major obstacle for SAXS, and descriptions of dedicated biological SAXS beamlines acknowledge the need to check for and avoid radiation damage (David & Pérez, 2009; Hura *et al.*, 2009; Pernot *et al.*, 2010; Blanchet *et al.*, 2012, 2015; Martel *et al.*, 2012; Nielsen *et al.*, 2012; Classen *et al.*, 2013; Kirby Mudie, Hawley, Cookson *et al.*, 2013; Kirby, Mudie, Hawley, Mertens *et al.*, 2013; Acerbo *et al.*, 2015). Minimizing radiation-induced changes in SAXS places limits on minimum sample volumes (~10 µl) and maximum X-ray exposure times (Dyer *et al.*, 2014; Skou *et al.*, 2014). Radiation damage is also an obstacle to time-resolved SAXS studies, as large amounts of sample must be available to obtain damage-free low-noise scattering profiles at many time points (Pollack, 2011; Graceffa *et al.*, 2013).

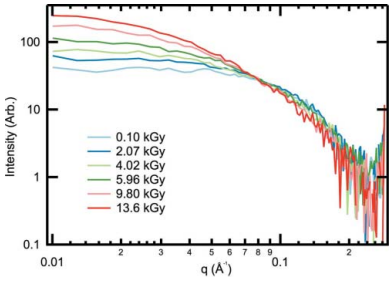

To minimize radiation damage, three strategies are commonly employed. First, exposure times for a test sample can be reduced until subsequent exposures of the test sample show no change in the scattering profile (Dyer *et al.*, 2014; Skou *et al.*, 2014). Second, the total sample volume irradiated can be increased, typically by flowing/oscillating the sample or defocusing the beam at the sample, to minimize dose (Fischetti *et al.*, 2003; Lipfert *et al.*, 2006; Classen *et al.*, 2013). Third, small-molecule compounds such as glycerol can be added to reduce changes in the SAXS profile (*e.g.* by competitively binding with free radicals or by inhibiting aggregation) (Kuwamoto *et al.*, 2004; Kmetko *et al.*, 2011; Bobrowski, 2012; Jeffries *et al.*, 2015). These approaches can be employed in parallel and result in the limitations on sample volume and exposure time given above. Cryocooling samples to 100 K has been shown to reduce radiation damage rates in SAXS (Meisburger *et al.*, 2013; Hopkins *et al.*, 2015), but substantial methodological development is required before cryocooling can be accepted for routine use. Despite the importance of radiation damage as a limiting factor in SAXS, early efforts using laboratory X-ray sources (Zipper & Durchschlag, 1980*a*,*b*,*c*, 1981; Zipper *et al.*, 1980, 1985; Zipper & Kriechbaum, 1986) have been followed by only two systematic, quantitative studies at synchrotron sources (Kuwamoto *et al.*, 2004; Jeffries *et al.*, 2015). With recent and planned upgrades to already bright third-generation sources and construction of high-brightness fourth-generation sources, understanding, quantifying and ultimately minimizing radiation damage in biological SAXS will be essential to efficient use and full exploitation of these sources.

To aid in the development of effective strategies for minimizing radiation damage, nominally identical experiments carried out by different experimenters or at different beamlines should yield identical results. Previous studies do not give a consistent framework for quantifying damage and neglect variables that may affect reported damage rates. For example, Meisburger *et al.* (2013) and Jeffries *et al.* (2015) use the same formula to calculate the absorbed X-ray energy, but differences in how they evaluate beam area would give, if everything else were equal, a factor of six difference in absorbed energy. Such discrepancies make the evaluation of claimed damage mitigation effects based on comparisons between independent studies very difficult.

Here we build upon previous work (Kuwamoto *et al.*, 2004; Meisburger *et al.*, 2013; Jeffries *et al.*, 2015) to develop a procedure for quantifying radiation damage in SAXS that is broadly applicable and allows comparison between different samples and beamlines. We discuss how to accurately quantify absorbed X-ray energy and dose (absorbed energy per unit mass of the sample) for static SAXS samples, accounting for variables including beam shape, diffusive exchange of protein into and out of the beam, and beam heating. Flowing or oscillating samples significantly complicate the calculation of dose, so we recommend and discuss in detail only static experiments. Different proteins show different modes of damage such that a single metric is insufficient to quantify radiation damage. We illustrate our procedure using radiation damage data for lysozyme, glucose isomerase and xylanase, which were collected at the MacCHESS BioSAXS user facility at the CHESS beamline G1 (Nielsen *et al.*, 2012; Acerbo *et al.*, 2015). Details of the data collection and processing methods are given in the supporting information (§S1); standard protocols for SAXS data collection and analysis have been previously reviewed (Dyer *et al.*, 2014; Skou *et al.*, 2014). Accurate quantification of dose and application of suitable damage metrics will facilitate development of methods to minimize radiation damage in SAXS.

2. Overview of a radiation damage experiment

The general steps recommended to quantify radiation damage in a static SAXS experiment are as follows:

(1) Calibration. Measure X-ray flux and beam shape at the sample position. Measure the path length through the sample, or the sample transmission. If necessary, measure or calculate sample density.

(2) Measurement. For each sample of interest, record consecutive exposures until clearly detectable damage is observed. For a given sample condition (protein concentration, buffer, temperature *etc.*), measure at least three identically prepared samples.

(3) Dose calculation. Calculate the X-ray dose for each exposure.

(4) Quantification. Calculate, at minimum, the following parameters for each scattering profile: radius of gyration, molecular weight and absolute integrated intensity. Normalize the parameters for a given sample to their initial values. Plot the normalized parameters *versus* dose.

(5) Damage sensitivity metrics. The resulting plots will generally have an initial linear region. Fit this region to obtain a radiation sensitivity per dose for each parameter.

If these steps are carried out as described below, data from different experiments and beamlines should be directly comparable. For radiation damage experiments that use non-static samples (particularly flowing samples), consecutive exposures may not be sufficient to increase the dose delivered to the sample. Other variables may need to be changed in step 2, such as flux density (by changing flux and/or beam size) or flow rate, to vary sample doses.

3. Definition of dose

Dose is the X-ray energy absorbed per unit mass of the sample, in units of Gray (Gy), where $1\ \mathrm{Gy} = 1\ \mathrm{J\ kg^{-1}}$. Radiation damage in most contexts is a strict function of dose (Holton, 2009). Dose is related to the number of absorbed or inelastically scattered photons, and for static samples is calculated as

$$\mathrm{Dose} = \frac{ftAE_\gamma}{\rho l}, \qquad (1)$$

where f is the flux density (ph $\mathrm{s^{-1}}$ $\mu\mathrm{m^{-2}}$), t is the exposure time, A is the fraction of incident energy absorbed, E_γ is the X-ray energy per photon, ρ is the sample density and l is the

X-ray path length through the sample (Kmetko *et al.*, 2006). For comparison between different experiments on the same beamline or between different beamlines, the number of incident photons and exposure time are not good proxies for dose. Dose can (and should) be calculated for non-static (such as flowing) samples, but different inputs will be needed to determine the absorbed energy and illuminated sample mass.

Accurately calculating the sample dose is critical for quantification of radiation damage. In macromolecular crystallography, tools for calculating dose (Murray *et al.*, 2005; Paithankar *et al.*, 2009; Paithankar & Garman, 2010; Zeldin *et al.*, 2013) are widely used in optimizing data collection. Such tools are not available for SAXS, and previous studies (Kuwamoto *et al.*, 2004; Meisburger *et al.*, 2013; Jeffries *et al.*, 2015) used different dose calculations.

4. Calibration of experiment and sample parameters

In order to accurately determine dose, the following experimental parameters must be known: buffer composition; macromolecule concentration; X-ray energy; exposure time; *flux and beam shape at the sample position*; *sample path length or sample transmission*; sample density; and the macromolecular diffusion coefficient in the buffer. The first four parameters are generally known for any SAXS experiment (Dyer *et al.*, 2014; Skou *et al.*, 2014), while the last two can be measured or calculated away from the beamline. The italicization indicates additional parameters not typically measured/reported for SAXS experiments that must be measured at the beamline for each experiment.

The beam shape at the sample position can be measured in a number of ways. These include detection of optical beam images (such as from fluorescence or scintillation); X-ray exposure of a glass slide followed by optical measurement of the resulting fogging (Meisburger *et al.*, 2013); and scanning a knife edge through the beam in perpendicular directions, measuring the flux downstream of the knife edge (for example on an active beamstop) and then calculating the derivative of the flux *versus* knife edge position. This latter method was used here, and details are given in Figs. S1 and S2.

The flux at the sample position can be measured by inserting a calibrated ion chamber or PIN diode at the sample position and then accounting for the attenuation of the upstream sample holder window. Alternatively, flux can be measured upstream or downstream of the sample, and the attenuation of any intervening material (such as windows on the downstream flight tube) can be calculated and accounted for. Here we measured the flux downstream of the vacuum flight tube and corrected for flight tube window attenuation using *XCOM* (Gerward *et al.*, 2001; Berger *et al.*, 2010). The sample path length can usually be obtained from a beamline scientist or by direct measurement of the sample holder. If it is unknown or not fixed, the transmission of a sample of known attenuation length (*e.g.* water) can be measured and used to estimate the path length, as done by Meisburger *et al.* (2013). As reported by Jeffries *et al.* (2015), sample densities can be calculated, for example by using *MULCh* (Whitten *et al.*, 2008), or measured. For solutions with modest protein, salt and buffering agent concentrations, the densities calculated using *MULCh* (Jeffries *et al.*, 2015) are within 3% of that of water, so using the density of water instead of the specific solution density will generally have a minimal effect on the dose calculation. Here we use the density of water, 1 g cm^{-3}.

5. Measurement of radiation damage data

In a static experiment (Kuwamoto *et al.*, 2004; Jeffries *et al.*, 2015), the sample is held stationary with respect to the X-ray beam and a series of SAXS images are recorded. Current detectors have minimal dead times between images, allowing continuous exposure with the X-ray shutter open for the experiment's duration and the most straightforward dose calculation. Detectors with significant dead times require beam shuttering between exposures. As we will discuss later, identically prepared samples do not yield identical damage rates, for reasons currently unknown. To account for this variability, at least three samples should be measured for a given set of sample conditions (sample concentration, buffer composition *etc.*).

It is useful to know what changes in a scattering profile might be expected as a result of radiation damage. The manifestations of radiation damage to macromolecules in solution are aggregation, fragmentation, conformation changes and unfolding, all of which can be detected by SAXS. The effect of aggregation on the scattering profile is well known: an increase in scattering at low q that produces a nonlinear Guinier region (Kuwamoto *et al.*, 2004; Jeffries *et al.*, 2015). It is also expected, though previously unreported, that aggregation will cause the scattering at high q to decrease. Fragmentation should cause the opposite, a decrease in scattering at low q and an increase at high q. Unfolding results in an increase in the radius of gyration, a decrease in the Porod exponent and an increase in flexibility with the accompanying characteristic changes in the Kratky and Porod–Debye plots (Rambo & Tainer, 2011). The effect of conformational changes on the scatter will depend on the particular changes.

Fig. 1 shows sample SAXS scattering profiles at increasing accumulated dose (calculated as described in §6) for lysozyme, xylanase and glucose isomerase, collected in static mode with continuous exposure. Both lysozyme and xylanase show an increase in intensity with dose at low q. This increase – the only previously reported effect of radiation damage in SAXS – is characteristic of aggregation: aggregates produce much more low-q scattering than the smaller protein molecules, and so even small quantities can be easily detected (Kuwamoto *et al.*, 2004; Skou *et al.*, 2014; Jeffries *et al.*, 2015). However, lysozyme also shows a decrease in intensity with dose at high q. This is also consistent with aggregation, as scattering from large particles decays to zero at lower q than that from small particles, although whether the amount of protein involved in aggregates is sufficient to explain the large-q intensity reduction [also possibly visible in Fig. 1(*b*) of Jeffries *et al.* (2015)] is unclear. In contrast, glucose isomerase shows a decrease in intensity with dose at low q, which could be characteristic of

fragmentation. The observed and expected responses of biomolecules to radiation, as manifested in their SAXS profiles, are thus quite diverse.

While commonly used to reduce radiation damage, flow/oscillation of the sample complicates the dose calculation. For typical flow cell diameters/widths (1.5–2 mm), flow rates (1–30 µl s^{-1}) (Martel *et al.*, 2012; Nielsen *et al.*, 2012; Kirby, Mudie, Hawley, Cookson *et al.*, 2013; Blanchet *et al.*, 2015; Jeffries *et al.*, 2015) and mean flow velocities (0.5–15 mm s^{-1}), the corresponding Reynolds numbers of between 1 and 25 are fully in the laminar flow regime. The expected Poiseuille velocity profile is parabolic with radial position r. For typical mean flow velocities and beam sizes (~500 µm), mean sample residence times in the beam of 0.03–1 s are too short for appreciable radial diffusive mixing (see §6.3 below.) Consequently, the Poiseuille profile results in radius-dependent biomolecule residence times in the X-ray beam. The resulting dose distribution within a flowing sample is nonuniform and depends on the geometry of the flow cell and the volume of the cell that is illuminated by X-rays. Similar behavior is expected in oscillating flow configurations. Static experiments are thus recommended for accurate quantification and comparison between beamlines. Once static radiation sensitivities are established, they can be used to estimate – and/or be directly compared with – damage in a flow/oscillation experiment. Even in static experiments, the sample plug may slowly creep or drift, bringing fresh sample into the beam; samples should be carefully observed or imaged before and after each measurement.

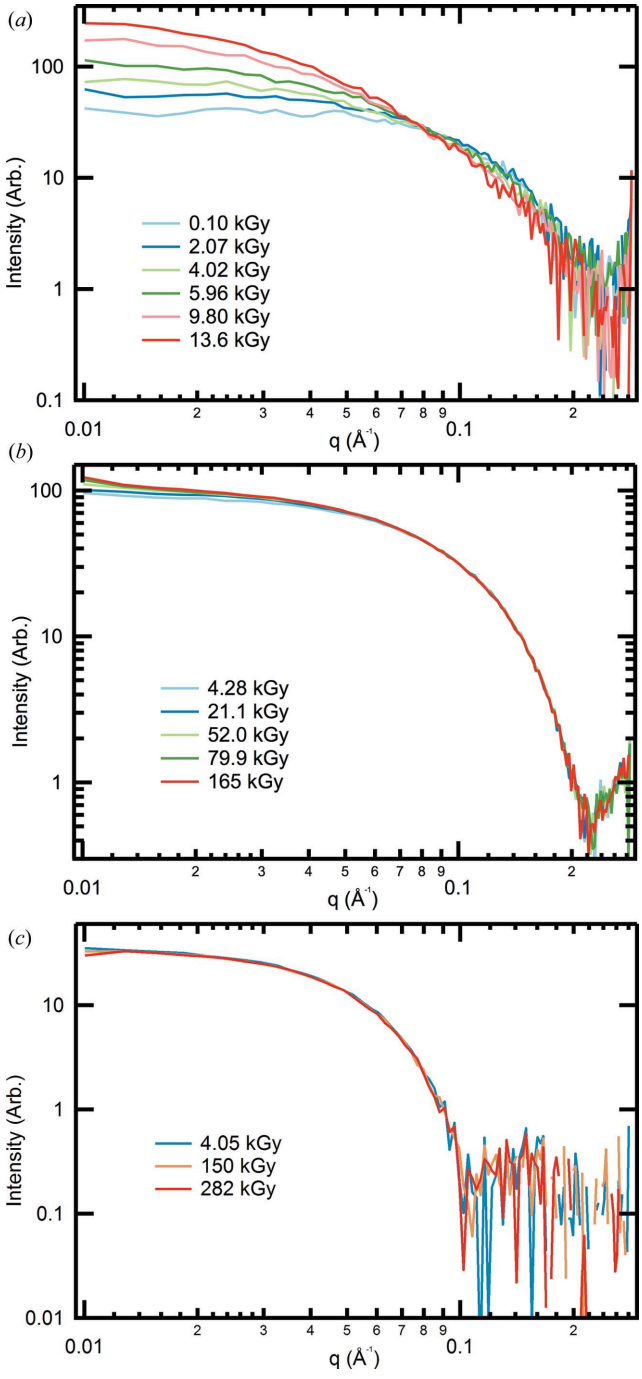

Figure 1
Selected scattering profiles of (*a*) 4.1 mg ml^{-1} lysozyme, (*b*) 4.9 mg ml^{-1} xylanase and (*c*) 1.2 mg ml^{-1} glucose isomerase as a function of dose. For lysozyme and xylanase, the damage manifests primarily as an increase in intensity at low q, indicating aggregation. For glucose isomerase, only a slight downturn is observed at the lowest q, which could be attributable to damage or charging.

6. Calculation of dose

Accurate calculation of dose using equation (1) requires accurate determination of all parameters. The flux density and absorbed energy fraction can be subject to a variety of corrections, as outlined below.

6.1. Determining the flux density

Flux density depends on beam shape (Zeldin *et al.*, 2013). For a robust metric of radiation-damage-induced change to the scattering profile, we need to consider not only the amount of damage caused to the sample at each position in the beam profile but also the magnitude of each position's contribution to the total SAXS signal. Sample regions where the flux density and thus damage are small also contribute little to the total scattering, and so should be appropriately weighted by the flux density when calculating dose. The appropriate weighted flux density $\overline{f}$ for use in equation (1) is given by

$$\overline{f} = \frac{\int f(x,y) f(x,y)\,\mathrm{d}A}{\int f(x,y)\,\mathrm{d}A}, \qquad (2)$$

where $f(x, y)$ is the beam profile perpendicular to the beam direction (z).

For a Gaussian beam,

$$f(x,y) = \frac{f_0}{(2\pi\sigma_x\sigma_y)^{1/2}} \exp\left[-\frac{1}{2}\left(\frac{x^2}{\sigma_x^2}+\frac{y^2}{\sigma_y^2}\right)\right], \qquad (3)$$

where f_0 is the total number of incident photons per second and σ_x and σ_y are the standard deviation of the Gaussian in x and y. Substituting this into equation (2) gives

$$\overline{f} = \frac{f_0}{4\pi\sigma_x\sigma_y}. \qquad (4)$$

The FWHM of a Gaussian is given by $2\sigma(2\ln 2)^{1/2}$, so the ratio of the flux density calculated by the FWHM method [$f_{\rm FWHM} = f_0/({\rm FWHM}_x{\rm FWHM}_y)$] and using equation (2) is

$$\frac{f_{\rm FWHM}}{\bar{f}} = \frac{\pi}{2\ln 2} \simeq 2.27. \quad (5)$$

This shows that accounting for the beam shape will apply a significant correction to the reported dose.

In the present work, $\bar{f}$ was numerically calculated using equation (2) and the measured beam profile. Meisburger *et al.* (2013) assumed that the incident photons were uniformly distributed within the FWHM; if their beam was Gaussian, this overestimated the dose by a factor of 2.3. Jeffries *et al.* (2015) assumed that the photons were uniformly distributed over the full extent of the beam (∼2.5 FWHM); if their beam was Gaussian, this underestimated the dose by a factor of 2.5.

6.2. Determining the absorbed energy fraction

In equation (1), the fraction of the incident energy that is absorbed, A, can be calculated from Beer's law:

$$A = 1 - \exp[-(\mu/\rho)\rho l], \quad (6)$$

where μ is an absorption coefficient and l is the sample path length. Absorption coefficients are tabulated as μ/ρ (Hubbell, 2006), where ρ is the sample density. Not all of the energy initially absorbed by the sample will stay within the volume of interest (the illuminated volume). The use of different absorption coefficients accounts for different energy loss mechanisms. A detailed discussion of absorption coefficients, given in §S2, shows that the mass photoelectric absorption coefficient, $\mu_{\rm pe}/\rho$, and the mass-energy absorption coefficient, $\mu_{\rm en}/\rho$, are both reasonable choices of absorption coefficients for SAXS. Further, at our energy of ∼10 keV, there is no difference between $\mu_{\rm pe}/\rho$ and $\mu_{\rm en}/\rho$ for water so either is acceptable. We chose to use $\mu_{\rm pe}/\rho$ to calculate the absorption, as it can be directly calculated for each sample condition using *XCOM* (Gerward *et al.*, 2001; Berger *et al.*, 2010). We note that the addition of buffer components and protein changes $\mu_{\rm pe}/\rho$ by only ∼1% (from 4.944 cm^2 g^{-1} for water to 5.008 cm^2 g^{-1} for 47.5 mg ml^{-1} lysozyme in buffer), so for our samples it would create minimal error to use the $\mu_{\rm pe}/\rho$ of water for every sample. If the path length of the sample is unknown, for example for the windowless sample holder used by Meisburger *et al.* (2013), the transmission can be used to approximate the path length as $l \simeq \mu^{-1}\ln(1/T)$. This can be used with equation (6) to estimate A.

6.3. Correcting for diffusive turnover

Equation (1) for dose assumes that all sample molecules within the X-ray beam are static. However, molecules will diffuse into and out of the illuminated volume, and also diffuse between regions having different flux densities within that volume. As with oscillating the sample, this will spread the energy absorbed from the beam over a larger volume, reducing the dose. The magnitude of this effect depends on the data collection time (and, in shuttered data collection, on the detector dead time between images), which determines maximum diffusion distances; the beam size, shape and intensity profile, which determine the distance molecules must diffuse to experience a substantially different flux density; and the molecular diffusion coefficient of the macromolecule in the buffer.

A timescale for this effect can be estimated by setting the average diffusion length $l = (Dt)^{1/2}$, where D is the diffusion coefficient, equal to half of the beam FWHM (or the smallest dimension for noncircular beams), as

$$t_{\rm d} = \frac{l^2_{\rm FWHM}}{4D}. \quad (7)$$

Since D is inversely proportional to a molecule's Stokes radius $R_{\rm s}$, $t_{\rm d} \propto R_{\rm s}$. For experiments on a given sample longer than $t_{\rm d}$ we expect diffusive turnover to be large. §S3 describes a more complete calculation to evaluate the dose correction to compensate for diffusion. This calculation shows that at $t_{\rm d}$ diffusion reduces the dose evaluated using equation (1) by a factor of 2. This validates $t_{\rm d}$ as a reasonable indicator of total exposure lengths for which diffusion effects will be important. For the SAXS data collected here for lysozyme, xylanase and glucose isomerase – using the measured beam size of 190 × 196 µm FWHM and maximum total exposure times of ∼3, 30 and 120 s, respectively (see §S1 for details) – the maximum diffusion corrections determined by the calculations in §S3 were 2.5, 35 and 43%, respectively.

The timescale for diffusion is proportional to $l^2_{\rm FWHM}$ and so rapidly becomes shorter as the beam size shrinks. For beams with FWHM = 100 and 10 µm, $t_{\rm d}$ = 20 and 0.2 s, respectively, for lysozyme. Fig. 2 shows how much diffusion reduces the dose, calculated as in §S3 relative to the expected dose without diffusion, for lysozyme irradiated by different beam sizes.

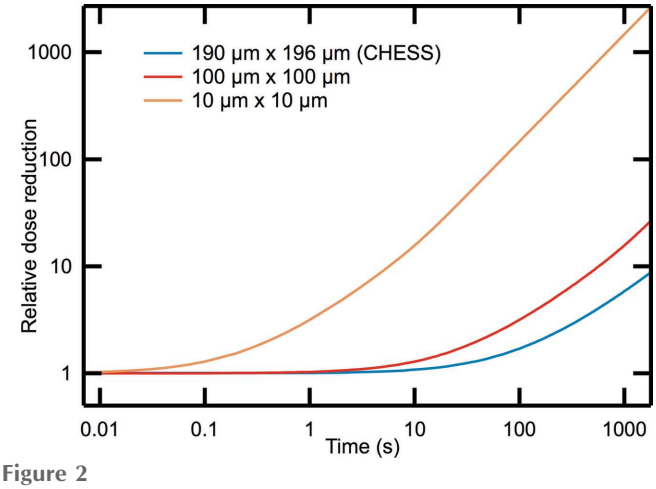

Figure 2
Dose reduction by diffusive exchange of lysozyme *versus* time for three beam sizes: 190 × 196 µm (used for the experiments in this paper), 100 × 100 µm and 10 × 10 µm. The vertical axis is the (unitless) factor by which diffusion reduces the dose, relative to the expected dose without diffusion. These reduction factors were calculated as described in §S3.

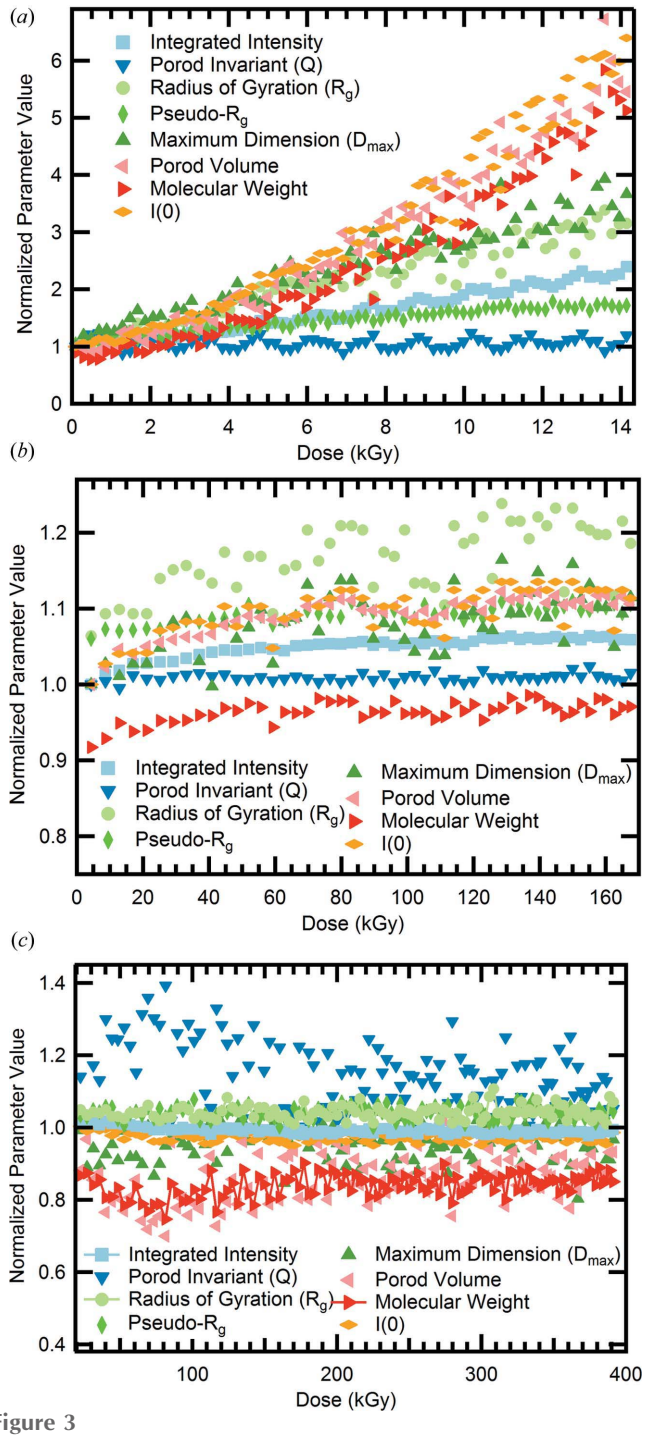

Figure 3
Plot of normalized calculated parameters *versus* dose for every scattering profile measured for single samples of (*a*) 4.1 mg ml^{-1} lysozyme, (*b*) 4.9 mg ml^{-1} xylanase and (*c*) 1.2 mg ml^{-1} glucose isomerase. For lysozyme and xylanase, every parameter except for the Porod invariant shows an increase with dose. For lysozyme, the integrated intensity, R_g and maximum dimension are linear for the entire dose range, while the Porod volume, molecular weight and $I(0)$ exhibit linear behavior only at doses below ~3 kGy. For xylanase, all of the increasing parameters show a relatively linear region for the first ~60 kGy. Unlike lysozyme and xylanase, for glucose isomerase most parameters remain roughly constant. An increase is clearly visible for the Porod invariant, while a similar decrease is visible for the Porod volume and molecular weight. It is not clear if the changes in the glucose isomerase sample are actually reflecting structural changes in the protein or are due to another effect such as charging.

7. Quantifying radiation damage data

7.1. Calculate parameters from scattering profiles, normalize

High-throughput SAXS beamlines are increasingly providing automated methods for assessing when radiation damage occurs (Pernot *et al.*, 2010; Blanchet *et al.*, 2015; De Maria Antolinos *et al.*, 2015). These methods use statistical techniques to determine when the measured scattering profile has significantly changed relative to the initial exposure (Franke *et al.*, 2012, 2015; Grant *et al.*, 2015). While practical for assessing the onset of radiation damage, these do not give data that can be easily interpreted as to type and rate of damage.

Almost any parameter that can be calculated from a SAXS profile can be used as a metric for radiation damage. Using a series of consecutive images, the parameter can be normalized by its value in the first image, and then plotted *versus* dose, yielding a 'dose curve'. Previously, metrics based on the change in the radius of gyration R_g, the pseudo radius of gyration and the scattering intensity at zero angle $I(0)$ were used to study radiation damage (Kuwamoto *et al.*, 2004; Jeffries *et al.*, 2015). We have investigated these and metrics based on additional parameters, including the Porod invariant, the Porod volume, the molecular weight, the maximum dimension and the integrated intensity. Details of these calculations are given in §S1.

Fig. 3 shows representative dose curves calculated from our sample data sets for lysozyme, xylanase and glucose isomerase, for these parameters. These dose curves show how radiation damage changes the information available from the SAXS scattering profile.

7.2. Calculate sensitivities from fits to dose curves

Dose curves generally show a linear region of change in parameter *versus* dose. The slope of the linear fit to the dose

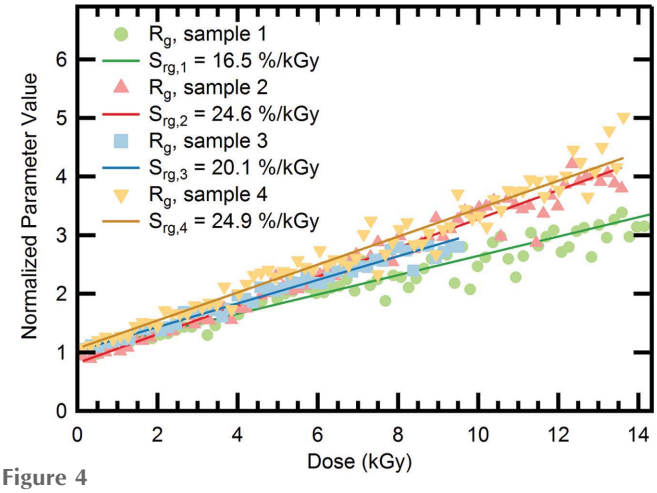

Figure 4
The change in normalized R_g as a function of dose for four identically prepared lysozyme samples. The lines represent the best linear fit and the values of the slopes are reported in the legend. For nominally identical samples, the sensitivities ranged from 16.5 to 24.9% kGy^{-1}, emphasizing the necessity of measuring and averaging sensitivities from multiple samples.

Table 1
R_g, molecular weight and integrated intensity sensitivities (S_{rg}, S_{mw} and S_I) and standard deviations (σ_{rg}, σ_{mw} and σ_I) for lysozyme (4.1 mg ml^{-1}), xylanase (4.9 mg ml^{-1}) and glucose isomerase (1.2 mg ml^{-1}).

Glucose isomerase shows radically different sensitivities, $S_{rg} \ll S_{mw}, S_I$, while for lysozyme and xylanase these sensitivities agree to within a factor of 2–3 or less.

Protein	Concentration (mg ml^{-1})	S_{rg} (% kGy^{-1})	σ_{rg} (% kGy^{-1})	S_{mw} (% kGy^{-1})	σ_{mw} (% kGy^{-1})	S_I (% kGy^{-1})	σ_I (% kGy^{-1})
Lysozyme	4.1	21.3	3.7	37.6	18.6	12.3	1.9
Xylanase	4.9	0.44	0.13	0.31	0.15	0.24	0.08
Glucose isomerase	1.2	−0.000046	0.0007	−0.10	0.08	−0.023	0.009

dependence of parameter P then gives the radiation sensitivity S_p. Most SAXS experiments deliver doses in the 1–10 kGy range, so % change per kGy provides a convenient unit allowing a quick estimate of damage in a typical experiment. Table 1 gives experimentally determined sensitivities for lysozyme (4.1 mg ml^{-1}), xylanase (4.9 mg ml^{-1}) and glucose isomerase (1.2 mg ml^{-1}), determined as described in §S4. Fig. 4 shows that identically prepared samples may exhibit different dose curves and different sensitivities. Consequently, it is important to measure at least three identically prepared samples, and report the average and standard deviation of the sensitivity. §S4 gives a detailed discussion of the behavior of these samples *versus* dose, including possible sources of sample-to-sample variability.

7.3. Which sensitivities are important?

Given the large number of possible parameters P, we would like to identify a minimal set that accurately captures the diverse radiation responses of biomolecules in SAXS. To do this, we calculated the Pearson product-moment correlation coefficient (Pearson's r) between every parameter P and for each SAXS data set, and then averaged the r values over all identically prepared samples. Example plots of these correlation coefficients for lysozyme, xylanase and glucose isomerase are shown in Figs. S3–S5. For lysozyme (Fig. S3), all of the parameters were strongly correlated ($r \geq 0.87$ for 4.1 mg ml^{-1} lysozyme) except for the Porod invariant. As seen in Fig. 3(*a*), the Porod invariant does not change for these samples, so in this case, any other parameter would characterize radiation damage in the system.

For xylanase (Fig. S4), there was less overall correlation. $I(0)$ correlated strongly with the integrated intensity and R_g ($r \simeq 0.84$), and both $I(0)$ and R_g correlated with the pseudo-R_g ($r \simeq 0.63$). The molecular weight correlated strongly with the Porod volume ($r = 0.93$). D_{max} correlated with R_g, $I(0)$ and the Porod volume ($r \simeq 0.7$), and the Porod invariant was correlated with the integrated intensity ($r = 0.68$). This suggests that the R_g, molecular weight and integrated intensity would serve as a minimal parameter set for examining damage.

For glucose isomerase, a significant change with dose was only seen in the integrated intensity, molecular weight, Porod volume and Porod invariant. Fig. S5 shows, as expected, that the molecular weight was strongly correlated with the Porod volume ($r = 0.94$), and both are strongly anticorrelated with the Porod invariant, ($r \simeq -0.95$). The integrated intensity was correlated with $I(0)$ ($r = 0.57$) but was otherwise not strongly correlated ($|r| \leq 0.42$) with anything. In this case molecular weight and integrated intensity would represent the damage.

Thus, for the proteins measured here, the radius of gyration, molecular weight and integrated intensity together capture the q-dependent changes in SAXS profiles with dose. R_g and molecular weight both provide insight into the structural changes caused by damage. Integrated intensity yields no obvious structural insight, but it is sensitive to any change in the scattering profile. Integrated intensity also has the advantage that it can be used to characterize radiation-induced changes in scatter from protein-free buffers. The integrated intensity will depend upon the q range and the instrument background and so will not typically be useful for comparison with results from separate experiments. For this work, the entire q range (see §S1) was used to calculate the integrated intensity. Note that the parameters used in previous work (Kuwamoto *et al.*, 2004; Jeffries *et al.*, 2015) – R_g and $I(0)$ – fail to capture the most important changes for glucose isomerase in Fig. 1(*c*).

In addition to the correlation analysis described above, principle component analysis was performed on the data, and this is described in §S5. The results of that analysis generally support the results of the correlation analysis, though the interpretation is not as straightforward. Further details of the correlation analysis are given in the same section.

7.4. Quantification in a nutshell

To summarize, first calculate the interesting parameters for each measured scattering profile. On the basis of our sample data, we recommend calculating, at minimum, the radius of gyration, molecular weight and integrated intensity. Second, normalize these parameters to the initial value and plot *versus* dose to generate dose curves. Third, fit the linear region of each dose curve to find the sensitivity of that parameter.

8. Additional considerations

The preceding sections provide the framework needed to reliably quantify radiation damage in SAXS, in a way that will allow comparison between different experiments and beamlines. This section will discuss experimental parameters that are either known to or may affect quantification, and so should be considered and reported for experiments. We will also discuss the idea of a critical dose, previously used as a metric for radiation damage.

8.1. Buffer composition, temperature, macromolecule concentration and degassing

Several additional factors could affect the radiation sensitivity measured by an experiment. The first of these is the

buffer composition. There is significant evidence that certain additives, such as glycerol or ascorbic acid, reduce the rate of damage in SAXS (Kuwamoto *et al.*, 2004; Jeffries *et al.*, 2015). Buffering agents and salts may also have an effect. For example, Tris scavenges OH radicals (Davies *et al.*, 1987; Audette-Stuart *et al.*, 2005) and may be a more effective radical scavenger than glycerol (Krisch *et al.*, 1991), while sodium nitrate scavenges aqueous electrons (Audette-Stuart *et al.*, 2005). Having identical buffers is thus important when attempting to study the effect of other experimental variables.

While temperature may nominally affect both macromolecule and radical diffusion rates, previous and present measurements (described in §S4) indicate that damage rates do not vary significantly between 277 and 303 K (Kuwamoto *et al.*, 2004; Jeffries *et al.*, 2015), although there is a huge reduction in damage rate on cooling to 100 K (Meisburger *et al.*, 2013). Protein concentration affects damage rate (Kuwamoto *et al.*, 2004; Jeffries *et al.*, 2015), so must also be properly controlled. Our data (§S4) show that a two orders of magnitude increase in lysozyme concentration reduces the measured sensitivities by a factor of ∼20.

It is sometimes mentioned that a deoxygenated environment or removal of dissolved oxygen from the solution can reduce radiation damage in SAXS (Hura *et al.*, 2009). Deoxygenating, or, more generally, degassing the solution, is also done to reduce the chance of bubble formation upon oscillation/flow, or to prevent the dissolved gasses from being forced out of solution when exposed to the X-ray beam (Kirby, Mudie, Hawley, Mertens *et al.*, 2013). In §S4 we report damage rates of degassed samples of lysozyme and xylanase. These degassed samples were damaged slightly faster than the normal samples. However, because of the large standard deviations involved, we cannot conclusively say there was any effect from degassing. The effect may be small, and it may also be protein and/or buffer dependent. Dissolved molecular oxygen in solution has been observed to both increase and decrease radiation sensitivity of macromolecules (Saha *et al.*, 1995). The assumed mechanism for sensitization is generation of superoxide radicals, O_2^{*-}, and singlet oxygen (Garrison, 1987), and reaction of these species with the macromolecules (Davies, 1987; Davies & Delsignore, 1987; Davies *et al.*, 1987). Sensitization by a factor of ∼2–3 has previously been observed (Saha *et al.*, 1995). When dissolved oxygen acts as a desensitizer, it is assumed to be as a result of scavenging of H^+ and e^-_{aq} by the oxygen in systems that are more sensitive to those species than the generated superoxide radicals (Garrison, 1987; Saha *et al.*, 1995).

8.2. X-ray energy and dose rate

X-ray energy and/or dose rate could affect the damage rate in SAXS samples. In X-ray crystallography, changing the X-ray energy does not change global damage rates (Murray *et al.*, 2005; Shimizu *et al.*, 2007), but there is some evidence from cryocooled samples that site-specific damage rates are affected (Homer *et al.*, 2011). Aggregation can be driven by site-specific damage, such as the reduction of surface cysteine residues and subsequent cross linking with cysteines on other molecules (Durchschlag & Zipper, 2007), and so might change with X-ray energy in SAXS. However, any energy dependence of site-specific damage to proteins in solution is likely to be much smaller than in protein crystals: in crystals, more protein damage is due to direct interaction with photoelectron-generated secondary electrons, whereas in dilute solution, most protein damage is due to interaction with radicals generated in the solvent.

For low dose rates (28–162 Gy s^{-1}), increasing the dose rate was found to increase the damage rate (Kuwamoto *et al.*, 2004), and this was attributed to diffusive turnover of the sample. It is unclear if there is an additional dose-rate effect once diffusion is accounted for.

8.3. Beam heating

Significant heating of macromolecules could lead to deleterious effects, such as denaturation, that could be mistaken for radiation damage. Beam heating could also create temperature gradients, driving convection and mixing that might reduce the apparent rate of damage. As discussed in §S6, we have estimated the heat diffusion timescale, the adiabatic heating rate, the adiabatic temperature rise ΔT_{ad}, the steady state temperature rise ΔT_{ss} (Warkentin *et al.*, 2012) and a minimum time to the onset of natural convection t^*. Table 2 gives values calculated using our experimental parameters and for several SAXS beamlines using parameters available online, which may not reflect the current state of the beamlines. Some beamlines may not use the maximum available flux for biological experiments, which would further reduce the calculated parameters. For our experiments, $\Delta T_{ad} = 0.08$ K, $\Delta T_{ss} = 0.13$ K and $t^* = 86$ s, so neither beam heating nor convection is expected to influence our results. The same appears true for current experiments on other SAXS beamlines.

8.4. Critical dose

Previous work has defined critical doses for radiation damage in SAXS (Kuwamoto *et al.*, 2004; Jeffries *et al.*, 2015). In the paper by Kuwamoto *et al.* (2004), the critical dose is somewhat imprecisely defined as the dose where damage is first observed. Jeffries *et al.* (2015) defined the critical dose as the dose at which the pseudo-R_g has changed by 0.1 nm. Applying the definition of Jeffries *et al.* (2015) to our glucose isomerase data, we find a critical dose of ∼66 000 kGy. However, the molecular weight shows a significant (∼13%) change after just ∼75 kGy. This suggests that one particular definition of a critical dose will not work for all proteins.

The critical dose for a system will depend upon the metrics/macromolecular properties of interest. For example, R_g is typically determined to a precision of ∼0.1–0.2 Å (in the best cases), which for lysozyme corresponds to a 1% change in R_g. One might then define the critical dose as that which causes a 1% change in R_g, which for our lysozyme data at concentrations near 4 mg ml^{-1} is ∼0.04–0.05 kGy. However, molecular weight is, as a rule of thumb, not determined in SAXS to better

Table 2
Estimates of beam heating at several BioSAXS beamlines.

All dose and heating rate calculations assume a sample composed of pure water. Dose calculations used equation (1), assuming the FWHM for a Gaussian beam. When the actual sample path length could not be found, a standard sample path length of 1.5 mm, indicated by an asterisk (*), was used. Calculations of t_d, δT_{ad}, ΔT_{ad}, ΔT_{ss} and t^* used the smallest beam dimension. Flux, beam size and energy numbers are from the following sources: BioCAT, measured April 2015; SIBYLS (Hura *et al.*, 2009); G1, measured (this paper); BL 4-2 (Martel *et al.*, 2012); ID02, assuming 200 mA ring current and sample path length 2 mm (ESRF, 2016*b*); BM29, assuming 1.8 mm path length (ESRF, 2016*a*); BL45XU (SPring-8, 2016); SAXS/WAXS (Australian Synchrotron, 2016); P12 (Jeffries *et al.*, 2015); I22 (Diamond, 2016); SWING (Synchrotron Soleil, 2016), path length from David & Pérez (2009). Some beamlines may not use the maximum available flux for biological experiments, further reducing the calculated parameters.

Beamline	Flux (ph s^{-1})	Beam size, FWHM (μm^2)	Energy (keV)	Sample path length (mm)	Dose rate (kGy s^{-1})	Adiabatic heating rate δT_{ad} (K s^{-1})	Adiabatic heat diffusion time t_d (s)	Adiabatic heating ΔT_{ad} (K)	Steady state heating ΔT_{ss} (K)	Time to onset of convection t^* (s)
BioCAT (APS)	1.1×10^{13}	115×122	12	1.5*	180	41	0.024	1	2	15
SIBYLS (ALS)	10^{12}	4000×1000	12	1.5*	0.05	0.01	1.8	0.02	8×10^{-5}	83
G1 – BioSAXS (MacCHESS)	9.6×10^{11}	190×196	9.96	2.0	5.1	1.2	0.06	0.08	0.1	86
BL 4-2 (SSRL)	2×10^{12}	300×500	11	1.5	3.2	0.8	0.16	0.1	0.2	46
ID02 (ESRF)	2×10^{14}	200×400	12.4	2	519	120	0.07	9	15	2.4
BM29 (ESRF)	10^{12}	700×700	12.5	1.8	0.43	0.10	0.88	0.09	0.03	80
BL45XU (SPring-8)	1×10^{12}	200×400	12.4	1.5*	2.8	0.7	0.07	0.05	0.08	77
SAXS/WAXS (Australian Synchrotron)	2×10^{13}	150×250	10	1.5	127	30	0.04	1	2	10
P12 (DESY)	4×10^{12}	110×200	10	1.7	39	9	0.02	0.2	0.5	31
I22 (Diamond)	6×10^{12}	320×80	12.4	1.5*	40	10	0.01	0.1	0.3	28
SWING (Synchrotron Soleil)	8×10^{12}	450×20	7	1.6	256	60	0.0007	0.04	0.2	16

than ∼10%, and our lysozyme data then give a dose limit of ∼0.2–0.3 kGy. The intrinsic 'noise' and precision limits on SAXS-derived parameters may vary between samples and beamlines, and these may also influence the choice of critical dose. For these reasons, we recommend using radiation sensitivities for each SAXS-derived parameter rather than a single critical dose, as they provide a more universal metric for damage rates.

9. Summary

Radiation damage in SAXS is a serious concern: it limits minimum sample volumes to ∼10 µl; it increases the need for frequent and aggressive cleaning of sample cells, slowing down data collection; and it requires extra data analysis in high-throughput experiments to ensure damage does not affect the results. The best strategies for reducing radiation damage remain oscillating or flowing the sample through the beam, to spread out the absorbed energy over a large volume (lowering the dose), and the addition of small-molecule compounds to the buffer to reduce damage (Fischetti *et al.*, 2003; Kuwamoto *et al.*, 2004; Lipfert *et al.*, 2006; Jeffries *et al.*, 2015). Additionally, cryocooling samples to 100 K can greatly reduce damage to the samples (Meisburger *et al.*, 2013; Hopkins *et al.*, 2015). As X-ray sources get brighter, with the upgrade of third-generation sources and the construction of fourth-generation sources, the need to prevent radiation damage will get more urgent. This paper builds upon previous literature to provide a protocol for accurate quantification of radiation damage in SAXS. This should enable accurate comparison of results between different beamlines and experiments, and so enable new studies of the most effective methods for reducing radiation damage.

The calculation of parameter radiation sensitivities could also provide initial static calibration measurements of molecule-specific radiation damage rates at beamlines. These rates could then be used to estimate radiation-damage-induced uncertainties in standard flow measurements based on the flow rates and biomolecule residence times in the X-ray beam. The challenge in this approach, as for the current techniques which detect radiation-damage-based statistically significant changes in the scattering profile (Franke *et al.*, 2012, 2015; Grant *et al.*, 2015), is determining what represents a significant change in the measurement of interest. The threshold for a significant change will depend not just on the statistical uncertainties inherent in the measurement and parameter determination, but also on the goals of the experiment, and so may need to be examined on a case by case basis.

10. Related literature

For additional literature relating to the supporting information, see Ambrosini *et al.* (2003), Boyd & Vest (1975), Butler *et al.* (1960), Davies (2012), Durchschlag *et al.* (2003), Fischer *et al.* (2010), Gillilan *et al.* (2013), Graewert & Svergun (2013), Huang *et al.* (1993), Hubbell (1999), Hubbell & Selter (2004), Kozak (2005, 2006), Kriminski *et al.* (2003), Kuzay *et al.* (2001), Lewis & Whitman (1924), Mylonas & Svergun (2007), Nielsen *et al.* (2009), Oberthuer *et al.* (2012), Parsons & Mulligan (1978), Petoukhov *et al.* (2007, 2012), Price *et al.* (1999), Rambo & Tainer (2013), Sanishvili *et al.* (2011), Vest & Lawson (1972), Voronov & Buleiko (1998), Winterbourn (2008), Witala *et al.* (2014) and Zhang *et al.* (2007).

Acknowledgements

This paper benefitted from discussions with Andrea M. Katz, Steve P. Meisburger, Matthew E. Warkentin and Lois Pollack about radiation damage and SAXS. Matthew E. Warkentin and Jonah Haber helped collect preliminary data (not used

here) that guided later data collection. Richard Gillilan is the staff scientist in charge of the MacCHESS BioSAXS user facility and aided with setup and data collection. He also provided the silver behenate calibrant. Arthur Woll is the beamline scientist for G-Line at CHESS and helped solve various instrumentation issues at the beamline. This work was funded by the NSF (DBI-1152348). This work is based upon research conducted at the Cornell High Energy Synchrotron Source (CHESS), which is supported by the National Science Foundation and the National Institutes of Health/National Institute of General Medical Sciences under NSF award DMR-0936384, using the Macromolecular Diffraction at CHESS (MacCHESS) facility, which is supported by award GM-103485 from the National Institutes of Health, through its National Institute of General Medical Sciences. This work made use of the Nanobiotechnology Center shared research facilities at Cornell.

References

Acerbo, A. S., Cook, M. J. & Gillilan, R. E. (2015). *J. Synchrotron Rad.* **22**, 180–186.
Ambrosini, D., Paoletti, D. & Schirripa Spagnolo, G. (2003). *Int. J. Heat Mass Transfer*, **46**, 4145–4155.
Audette-Stuart, M., Houée-Levin, C. & Potier, M. (2005). *Radiat. Phys. Chem.* **72**, 301–306.
Australian Synchroton (2016). *SAXS Beamline Technical Specifications*, http://www.synchrotron.org.au/aussyncbeamlines/saxswaxs/saxs-specifications.
Berger, M. J., Hubbell, J. H., Seltzer, S. M., Chang, J., Coursey, J. S., Sukumar, R., Zucker, D. S. & Olsen, K. (2010). *XCOM: Photon Cross Sections Database (Version 1.5)*, http://www.nist.gov/pml/data/xcom/index.cfm.
Blanchet, C. E., Spilotros, A., Schwemmer, F., Graewert, M. A., Kikhney, A., Jeffries, C. M., Franke, D., Mark, D., Zengerle, R., Cipriani, F., Fiedler, S., Roessle, M. & Svergun, D. I. (2015). *J. Appl. Cryst.* **48**, 431–443.
Blanchet, C. E., Zozulya, A. V., Kikhney, A. G., Franke, D., Konarev, P. V., Shang, W., Klaering, R., Robrahn, B., Hermes, C., Cipriani, F., Svergun, D. I. & Roessle, M. (2012). *J. Appl. Cryst.* **45**, 489–495.
Bobrowski, K. (2012). *Encyclopedia of Radicals in Chemistry, Biology, and Materials*, edited by C. Chatgilialoglu & A. Studer, pp. 395–432. Hoboken: John Wiley and Sons.
Boyd, R. D. & Vest, C. M. (1975). *Appl. Phys. Lett.* **26**, 287–288.
Butler, J. A. V., Robins, A. B. & Rotblat, J. (1960). *Proc. R. Soc. A Math. Phys. Eng. Sci.* **256**, 1–14.
Classen, S., Hura, G. L., Holton, J. M., Rambo, R. P., Rodic, I., McGuire, P. J., Dyer, K., Hammel, M., Meigs, G., Frankel, K. A. & Tainer, J. A. (2013). *J. Appl. Cryst.* **46**, 1–13.
David, G. & Pérez, J. (2009). *J. Appl. Cryst.* **42**, 892–900.
Davies, K. J. A. (1987). *J. Biol. Chem.* **262**, 9895–9901.
Davies, M. J. (2012). *Encyclopedia of Radicals in Chemistry, Biology and Materials*, edited by C. Chatgilialoglu & A. Studer, pp. 1425–1457. Hoboken: John Wiley and Sons.
Davies, K. J. A. & Delsignore, M. E. (1987). *J. Biol. Chem.* **262**, 9908–9913.
Davies, K. J. A., Delsignore, M. E. & Lin, S. W. (1987). *J. Biol. Chem.* **262**, 9902–9907.
De Maria Antolinos, A., Pernot, P., Brennich, M. E., Kieffer, J., Bowler, M. W., Delageniere, S., Ohlsson, S., Malbet Monaco, S., Ashton, A., Franke, D., Svergun, D., McSweeney, S., Gordon, E. & Round, A. (2015). *Acta Cryst.* D**71**, 76–85.
Diamond (2016). *Technical Specifications – I22 – Small Angle Scattering Beamline*, http://www.diamond.ac.uk/Beamlines/Soft-Condensed-Matter/small-angle/I22/specs.html.
Durchschlag, H., Hefferle, T. & Zipper, P. (2003). *Radiat. Phys. Chem.* **67**, 479–486.
Durchschlag, H. & Zipper, P. (2007). *Radiat. Phys. Chem.* **76**, 1295–1301.
Dyer, K. N., Hammel, M., Rambo, R. P., Tsutakawa, S. E., Rodic, I., Classen, S., Tainer, J. A. & Hura, G. L. (2014). *Structural Genomics: General Applications*, edited by Y. W. Chen, pp. 245–258. Totowa: Humana Press.
ESRF (2016*a*). *BM29 Beamline Specification*, http://www.esrf.eu/home/UsersAndScience/Experiments/MX/About_our_beamlines/bm29/beamline-specifications.html.
ESRF (2016*b*). *ID02 Beamline Layout*, http://www.esrf.eu/home/UsersAndScience/Experiments/CBS/ID02/BeamlineLayout.html.
Fischer, H., de Oliveira Neto, M., Napolitano, H. B., Polikarpov, I. & Craievich, A. F. (2010). *J. Appl. Cryst.* **43**, 101–109.
Fischetti, R. F., Rodi, D. J., Mirza, A., Irving, T. C., Kondrashkina, E. & Makowski, L. (2003). *J. Synchrotron Rad.* **10**, 398–404.
Franke, D., Jeffries, C. M. & Svergun, D. I. (2015). *Nat. Methods*, **12**, 419–422.
Franke, D., Kikhney, A. G. & Svergun, D. I. (2012). *Nucl. Instrum. Methods Phys. Res. Sect. A*, **689**, 52–59.
Garrison, W. M. (1987). *Chem. Rev*. **87**, 381–398.
Gerward, L., Guilbert, N., Bjørn Jensen, K. & Levring, H. (2001). *Radiat. Phys. Chem.* **60**, 23–24.
Gillilan, R. E., Cook, M., Temnykh, G., Møller, M. & Nielsen, S. (2013). *Am. Crystallogr. Assoc. Trans.* **2013**, 40–50.
Graceffa, R., Nobrega, R. P., Barrea, R. A., Kathuria, S. V., Chakravarthy, S., Bilsel, O. & Irving, T. C. (2013). *J. Synchrotron Rad.* **20**, 820–825.
Graewert, M. A. & Svergun, D. I. (2013). *Curr. Opin. Struct. Biol.* **23**, 748–754.
Grant, T. D., Luft, J. R., Carter, L. G., Matsui, T., Weiss, T. M., Martel, A. & Snell, E. H. (2015). *Acta Cryst.* D**71**, 45–56.
Holton, J. M. (2009). *J. Synchrotron Rad.* **16**, 133–142.
Homer, C., Cooper, L. & Gonzalez, A. (2011). *J. Synchrotron Rad.* **18**, 338–345.
Hopkins, J. B., Katz, A. M., Meisburger, S. P., Warkentin, M. A., Thorne, R. E. & Pollack, L. (2015). *J. Appl. Cryst.* **48**, 227–237.
Huang, T. C., Toraya, H., Blanton, T. N. & Wu, Y. (1993). *J. Appl. Cryst.* **26**, 180–184.
Hubbell, J. H. (1999). *Phys. Med. Biol.* **44**, R1–22.
Hubbell, J. H. (2006). *Phys. Med. Biol.* **51**, R245–R262.
Hubbell, J. H. & Selter, S. M. (2004). *Tables of X-ray Mass Attenuation Coeficients and Mass Energy-Absorption Coefficients from 1 keV to 20 MeV for Elements Z = 1 to 92 and 48 Additional Substances of Dosimetric Interest*, http://www.nist.gov/pml/data/xraycoef/.
Hura, G. L., Menon, A. L., Hammel, M., Rambo, R. P., Poole, F. L. II, Tsutakawa, S. E., Jenney, F. E. Jr, Classen, S., Frankel, K. A., Hopkins, R. C., Yang, S., Scott, J. W., Dillard, B. D., Adams, M. W. W. & Tainer, J. A. (2009). *Nat. Methods*, **6**, 606–612.
Jeffries, C. M., Graewert, M. A., Svergun, D. I. & Blanchet, C. E. (2015). *J. Synchrotron Rad.* **22**, 273–279.
Kirby, N. M., Mudie, S. T., Hawley, A. M., Cookson, D. J., Mertens, H. D. T., Cowieson, N. & Samardzic-Boban, V. (2013). *J. Appl. Cryst.* **46**, 1670–1680.
Kirby, N., Mudie, S., Hawley, A., Mertens, H. D. T., Cowieson, N., Samardzic Boban, V., Felzmann, U., Mudie, N. & Dwyer, J. (2013). *Am. Crystallogr. Assoc. Trans*. **2013**, 27–39.
Kmetko, J., Husseini, N. S., Naides, M., Kalinin, Y. & Thorne, R. E. (2006). *Acta Cryst.* D**62**, 1030–1038.
Kmetko, J., Warkentin, M., Englich, U. & Thorne, R. E. (2011). *Acta Cryst.* D**67**, 881–893.
Kozak, M. (2005). *J. Appl. Cryst.* **38**, 555–558.
Kozak, M. (2006). *Biopolymers*, **83**, 95–102.
Kriminski, S., Kazmierczak, M. & Thorne, R. E. (2003). *Acta Cryst.* D**59**, 697–708.
Krisch, R. E., Flick, M. B. & Trumbore, C. N. (1991). *Radiat. Res.* **126**, 251–259.

Kuwamoto, S., Akiyama, S. & Fujisawa, T. (2004). *J. Synchrotron Rad.* **11**, 462–468.
Kuzay, T. M., Kazmierczak, M. & Hsieh, B. J. (2001). *Acta Cryst.* D**57**, 69–81.
Lewis, W. K. & Whitman, W. G. (1924). *Ind. Eng. Chem.* **16**, 1215–1220.
Lipfert, J., Millett, I. S., Seifert, S. & Doniach, S. (2006). *Rev. Sci. Instrum.* **77**, 046108.
Martel, A., Liu, P., Weiss, T. M., Niebuhr, M. & Tsuruta, H. (2012). *J. Synchrotron Rad.* **19**, 431–434.
Meisburger, S. P., Warkentin, M., Chen, H., Hopkins, J. B., Gillilan, R. E., Pollack, L. & Thorne, R. E. (2013). *Biophys. J.* **104**, 227–236.
Murray, J. W., Rudiño-Piñera, E., Owen, R. L., Grininger, M., Ravelli, R. B. G. & Garman, E. F. (2005). *J. Synchrotron Rad.* **12**, 268–275.
Mylonas, E. & Svergun, D. I. (2007). *J. Appl. Cryst.* **40**, s245–s249.
Nielsen, S. S., Møller, M. & Gillilan, R. E. (2012). *J. Appl. Cryst.* **45**, 213–223.
Nielsen, S. S., Toft, K. N., Snakenborg, D., Jeppesen, M. G., Jacobsen, J. K., Vestergaard, B., Kutter, J. P. & Arleth, L. (2009). *J. Appl. Cryst.* **42**, 959–964.
Oberthuer, D., Melero-García, E., Dierks, K., Meyer, A., Betzel, C., Garcia-Caballero, A. & Gavira, J. A. (2012). *PLoS One*, **7**, e33545.
Paithankar, K. S. & Garman, E. F. (2010). *Acta Cryst.* D**66**, 381–388.
Paithankar, K. S., Owen, R. L. & Garman, E. F. (2009). *J. Synchrotron Rad.* **16**, 152–162.
Parsons, J. R. Jr & Mulligan, J. C. (1978). *J. Heat Transfer*, **100**, 423–428.
Pernot, P., Theveneau, P., Giraud, T., Fernandes, R. N., Nurizzo, D., Spruce, D., Surr, J., McSweeney, S., Round, A., Felisaz, F., Foedinger, L., Gobbo, A., Huet, J., Villard, C. & Cipriani, F. (2010). *J. Phys. Conf. Ser.* **247**, 012009.
Petoukhov, M. V., Franke, D., Shkumatov, A. V., Tria, G., Kikhney, A. G., Gajda, M., Gorba, C., Mertens, H. D. T., Konarev, P. V. & Svergun, D. I. (2012). *J. Appl. Cryst.* **45**, 342–350.
Petoukhov, M. V., Konarev, P. V., Kikhney, A. G. & Svergun, D. I. (2007). *J. Appl. Cryst.* **40**, s223–s228.
Pollack, L. (2011). *Biopolymers*, **95**, 543–549.
Price, W. S., Tsuchiya, F. & Arata, Y. (1999). *J. Am. Chem. Soc.* **121**, 11503–11512.
Rambo, R. P. & Tainer, J. A. (2011). *Biopolymers*, **95**, 559–571.
Rambo, R. P. & Tainer, J. A. (2013). *Nature*, **496**, 477–481.
Saha, A., Mandal, P. C. & Bhattacharyya, S. N. (1995). *Radiat. Phys. Chem.* **46**, 123–145.
Sanishvili, R., Yoder, D. W., Pothineni, S. B., Rosenbaum, G., Xu, S., Vogt, S., Stepanov, S., Makarov, O. A., Corcoran, S., Benn, R., Nagarajan, V., Smith, J. L. & Fischetti, R. F. (2011). *Proc. Natl Acad. Sci. USA*, **108**, 6127–6132.
Shimizu, N., Hirata, K., Hasegawa, K., Ueno, G. & Yamamoto, M. (2007). *J. Synchrotron Rad.* **14**, 4–10.
Skou, S., Gillilan, R. E. & Ando, N. (2014). *Nat. Protoc.* **9**, 1727–1739.
SPring-8 (2016). *BL45XU Outline*, http://www.spring8.or.jp/wkg/BL45XU/instrument/lang-en/INS-0000000334/instrument_summary_view.
Synchrotron Soleil (2016). *SWING beamline*, http://www.synchrotron-soleil.fr/Recherche/LignesLumiere/SWING#TechnicalData.
Vest, C. M. & Lawson, M. L. (1972). *Int. J. Heat Mass Transfer*, **15**, 1281–1283.
Voronov, V. P. & Buleiko, V. M. (1998). *J. Exp. Theor. Phys.* **86**, 586–590.
Warkentin, M., Badeau, R., Hopkins, J. B., Mulichak, A. M., Keefe, L. J. & Thorne, R. E. (2012). *Acta Cryst.* D**68**, 124–133.
Whitten, A. E., Cai, S. & Trewhella, J. (2008). *J. Appl. Cryst.* **41**, 222–226.
Winterbourn, C. C. (2008). *Nat. Chem. Biol.* **4**, 278–286.
Witala, M., Han, J., Menzel, A. & Nygård, K. (2014). *J. Appl. Cryst.* **47**, 2078–2080.
Zeldin, O. B., Gerstel, M. & Garman, E. F. (2013). *J. Appl. Cryst.* **46**, 1225–1230.
Zhang, F., Skoda, M. W. A., Jacobs, R. M. J., Martin, R. A., Martin, C. M. & Schreiber, F. (2007). *J. Phys. Chem. B*, **111**, 251–259.
Zipper, P. & Durchschlag, H. (1980*a*). *Z. Naturforsch. Teil. C*, **35**, 890–901.
Zipper, P. & Durchschlag, H. (1980*b*). *Radiat. Environ. Biophys.* **18**, 99–121.
Zipper, P. & Durchschlag, H. (1980*c*). *Monatsh. Chem.* **111**, 1367–1390.
Zipper, P. & Durchschlag, H. (1981). *Monatsh. Chem.* **112**, 1–23.
Zipper, P., Gatterer, H. G., Schurz, J. & Durchschlag, H. (1980). *Monatsh. Chem.* **111**, 981–1004.
Zipper, P. & Kriechbaum, M. (1986). *Monatsh. Chem.* **117**, 557–572.
Zipper, P., Wilfing, R., Kriechbaum, M. & Durchschlag, H. (1985). *Z. Naturforsch. Teil C*, **40**, 364–372.